Surrogate Assisted Radome Design: Preliminary Analysis

M. Salucci, G. Oliveri, M. A. Hannan and A. Massa

Contents

1 Glossary and Definitions

1.1 Parameters of the optimization

1.1.1 General Parameters

- K: Dimension of the input space (i.e., the number of variables);
- P: Population size;
- $\Phi\left(\mathbf{x}_p^{(i)}\right)$: real fitness associated to individual p at iteration i-th;
- $\tilde{\Phi}\left(\mathbf{x}_p^{(i)}\right)$: predicted fitness associated to individual p at iteration i-th;

1.1.2 SADE Parameters

- Q: DE scaling factor;
- τ: Dimension of the training set built at each $SADE$ iteration;
- i: Iteration index;
- $D^{(i)}$: Dimension of the database of simulated individuals at iteration i-th;
- $s^2\left\{\tilde{\Phi}\left(\mathbf{x}_p^{(i)}\right)\right\}$: Kriging prediction uncertainty (MSE) associated to prediction $\tilde{\Phi}\left(\mathbf{x}_p^{(i)}\right)$;
- ω: "*exploration*" parameter for the Lower Confidence Bound (LCB) pre-screening method;
- $Y(.)$: Cumulative distribution function of the standard normal distribution

$$Y(x) = \frac{1}{2} erf\left(\frac{x}{\sqrt{2}}\right) + \frac{1}{2} \tag{1}$$

where

$$erf(x) = \frac{2}{\sqrt{\pi}} \int_0^x e^{-t^2} dt \tag{2}$$

- $y(.)$: Probability density function of the standard normal distribution

$$y(x) = \frac{1}{\sqrt{2\pi}} e^{-\frac{x^2}{2}} \tag{3}$$

1.2 Prediction errors definition

Let be defined the following quantities:

- $\hat{y}_m$: predicted value associated to the m-th test sample;
- y_m: true value associated to the m-th test sample;
- M: number of test samples (size of the test set);
- $\bar{y}$: average of the true values associated to M test samples.

The following error metrics are defined and used hereinafter to evaluate the accuracy of a given predictor:

1. **Mean Absolute Error** (MAE)

$$MAE = \frac{1}{M}\sum_{m=1}^{M}|\hat{y}_m - y_m|$$

2. **Normalized Mean Error** (NME)

$$NME = \frac{1}{M}\sum_{m=1}^{M}\frac{|\hat{y}_m - y_m|}{|y_m|}$$

3. **Mean Squared Error** (MSE) [(1)]

$$MSE = \frac{1}{M}\sum_{m=1}^{M}(\hat{y}_m - y_m)^2$$

4. **Root Mean Squared Error** ($RMSE$)

$$RMSE = \sqrt{MSE}$$

5. **Normalized Root Mean Squared Error** ($NRMSE$)

$$NRMSE = \sqrt{\frac{\sum_{m=1}^{M}(\hat{y}_m - y_m)^2}{\sum_{m=1}^{M}(y_m)^2}}$$

6. **Normalized Maximum Error** ($NEMAX$)

$$NEMAX = \frac{\max_{m=1,\dots,M}\{|\hat{y}_m - y_m|\}}{\sqrt{\frac{1}{M}\sum_{m=1}^{M}(y_m - \bar{y})^2}}$$

[(1)] **NOTE:** This doesn't correspond to the definition of the Kriging MSE (prediction uncertainty)!

7. **Matching Error** (ME)

$$ME = \frac{\sum_{m=1}^{M} |\hat{y}_m - y_m|^2}{\sum_{m=1}^{M} |y_m|^2}$$

8. **Variance-Normalized Mean Squared Error** ($VNMSE$)

$$VNMSE = \frac{MSE}{Var\left(\{y_m\}\right)} = \frac{\frac{1}{M}\sum_{m=1}^{M}\left(\hat{y}_m - y_m\right)^2}{\frac{1}{M}\sum_{m=1}^{M}\left(y_m - \bar{y}\right)^2} = \frac{\sum_{m=1}^{M}\left(\hat{y}_m - y_m\right)^2}{\sum_{m=1}^{M}\left(y_m - \bar{y}\right)^2}$$

1.3 Time saving definition

Let us assume that our goal is to evaluate a given cost function in S user-defined samples. We can proceed in two ways:

1. Evaluate the S samples by using a full wave simulator.
2. Evaluate the S samples by using a predictor. In this case, we will have
   (a) $N < S$ simulations using the full wave simulator, to build the training set;
   (b) $M = (S - N)$ evaluations using the trained predictor.

The time saving using the predictor instead of computing all the S samples with the simulator is defined as

$$\Delta t^{saving}(N) = \left(\frac{\Delta t^{sim}_{tot} - \Delta t^{pred}_{tot}(N)}{\Delta t^{sim}_{tot}} \right) \tag{4}$$

where

- $\Delta t^{sim}_{tot} = S \times \Delta t^{sim}$: time required to simulate S samples using the e.m. simulator;
- Δt^{sim} is the average time required to perform a single e.m. simulation;
- $\Delta t^{pred}_{tot}(N) = \left(N \times \Delta t^{sim}\right) + \Delta t^{train}(N) + M \times \Delta t^{test}(N)$: time required if the predictor is used to estimate the value of the cost function in $M = (S - N)$ samples;
  - $N \times \Delta t^{sim}$: time required to generate the training set for the predictor made of N training samples;
  - $\Delta t^{train}(N)$: time required to train the predictor using N training samples;
  - $\Delta t^{test}(N)$: time required by the predictor to predict a single function value when trained with N training samples.

1.3.1 Incremental training generation with random selection from S samples

1. Randomly select N_1 training samples from the S available input-output pairs (e.g., an LHS training set);
2. Train a predictor using the selected training samples;
3. Predict the remaining $M_1 = (S - N_1)$ samples and compute the associate prediction error;
4. Randomly select new ΔN samples from S and add them to the previous training set ($N_2 = N_1 + \Delta N$). The test set now contains the remaining $M_2 = (S - N_2)$ sites;
5. Go to 2, iterate until the selected maximum training dimension is considered to train the predictor (note that $N_{max} < S$, in order to have some test samples on which evaluate the prediction accuracy).

1.4 Ogive radome shape

In the following report, the $3D$ ogive radome surface is modeled by using the superspheroidal surface for the unified description of a wide range of airborne radome shapes. The surface of a superspheroidal body is given by the equation

$$x^2 + y^2 \quad = \quad \left(\frac{D}{2L}\right)^2 (L^\nu - z^\nu)^{2/\nu}, \ z \in [0, L] \tag{5}$$

where

- D: base diameter of the radome;
- L: length of the radome;
- ν: parameter associated to the curvature of the radome ($\nu \in [1, 2]$);

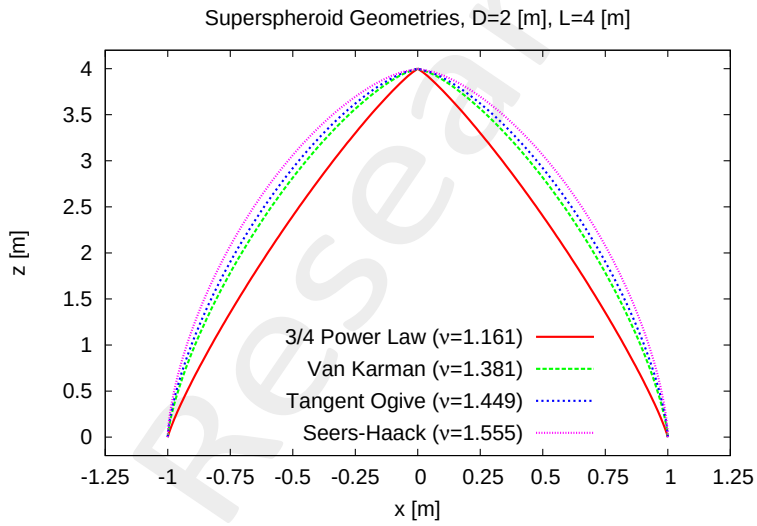

Figure 1: Plot of the ogive shapes.

1.4.1 Multilayer radome

The volume Ω_n associated to the n-th layer with thickness t_n of a N layers ogive radome is defined as

$$\Omega_n \quad = \quad \Omega'_{n-1} \backslash \Omega'_n, \ n = 1, ..., N \tag{6}$$

where

$$\Omega'_n \quad = \quad \left\{ (x, y, z) \in \mathbb{R}^3 | x^2 + y^2 \leq \left(\frac{D_n}{2L_n}\right)^2 (L_n^\nu - z^\nu)^{2/\nu}, \ z \in [0, L_n] \right\}, \ n = 0, .., N \tag{7}$$

and

$$D_n = \begin{cases} D & \text{if } n = 0 \\ D - 2\sum_{n=1}^{N} t_n & \text{if } n > 0 \end{cases}, \; n = 0, ..., N \tag{8}$$

$$L_n = \begin{cases} L & \text{if } n = 0 \\ L - \sum_{n=1}^{N} t_n & \text{if } n > 0 \end{cases}, \; n = 0, ..., N \tag{9}$$

The operand \ denotes the subtraction of the volume Ω'_n from the volume Ω'_{n-1}.

1.4.2 Spline-Based Radome Thickness Profile

The external surface of the radome is modeled by means of the Equation (5), while the thickness profile of the structure is modeled with a spline, as shown in Figure (2).

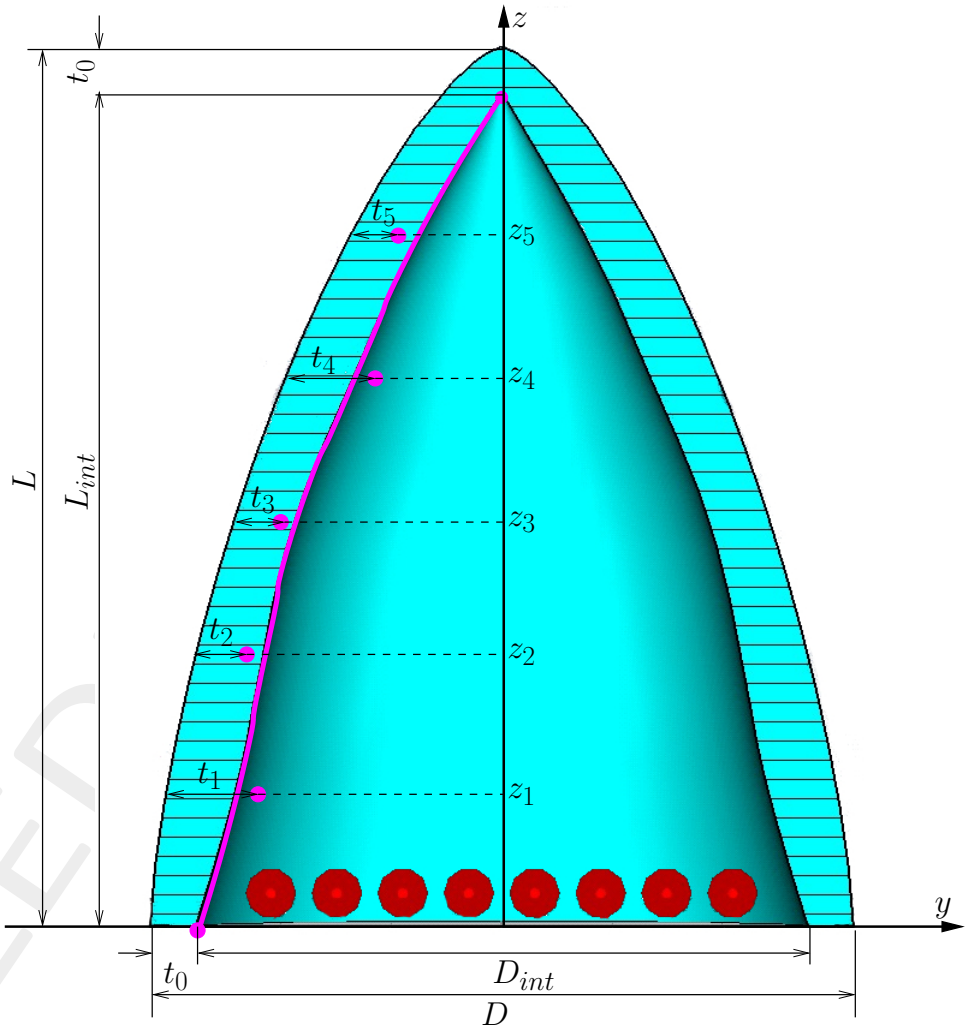

Figure 2: Plot of the ogive-shaped radome with spline thickness profile.

1.4.3 Quadratic Bezier curve: Definition

Let be given

- Q: number of control points;
- $\left(P_x^{(q)}, P_y^{(q)}\right)$: coordinates of the q-th control point;

A Bezier quadratic spline interpolating the Q control points is built as follows

1. Compute the coordinates of the Q virtual points. The $q-th$ virtual point is located in the middle of the line between the two control points q and $q+1$, and its coordinates are given by

$$V_x^{(q)} = \frac{P_x^{(q)} + P_x^{(q+1)}}{2}$$

$$V_y^{(q)} = \frac{P_y^{(q)} + P_y^{(q+1)}}{2}$$

2. For each control point $(q = 1, ..., Q)$ draw a quadratic curve by considering its two adjacent virtual points. The curve for the control point q is defined as

$$B_x^{(q)}(t) = \left(1 - t^2\right) V_x^{(q)} + 2t\,(1-t)\,P_x^{(q)} + t^2 V_x^{(q+1)}$$

$$B_y^{(q)}(t) = \left(1 - t^2\right) V_y^{(q)} + 2t\,(1-t)\,P_y^{(q)} + t^2 V_y^{(q+1)}$$

   for $t \in [0, 1]$.

3. Join the q segments to form the full interpolating spline curve.

Example

The following figure shows the computed spline for $Q = 5$ control points defined in table I. Note that the spline curve doesn't pass through any of the selected control points.

Index	Control Points $\left(P_x^{(q)}, P_y^{(q)}\right)$	Virtual Points $\left(V_x^{(q)}, V_y^{(q)}\right)$
1	$(3, 5)$	$(4, 4)$
2	$(5, 3)$	$(4.5, 2)$
3	$(4, 1)$	$(3.5, 2)$
4	$(3, 3)$	$(2, 3.5)$
5	$(1, 4)$	$(2, 4.5)$

Table I: Location of the control points and of the virtual points.

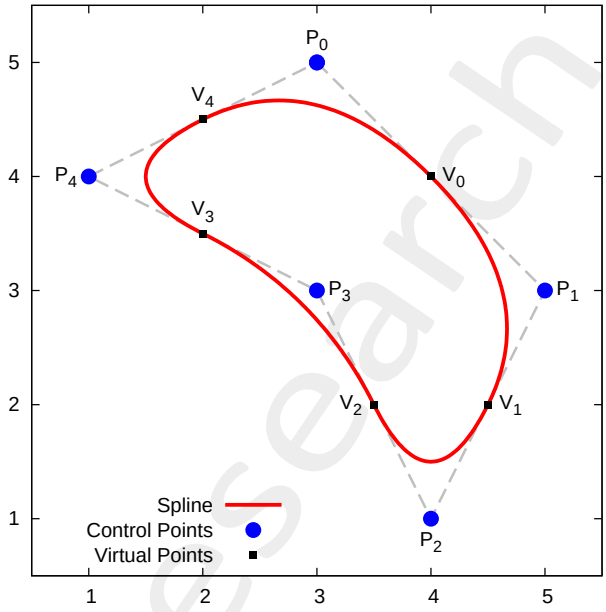

Figure 3: Plot of a quadratic spline passing through the selected control points.

2 Radome effect analysis

This aim of this section is the validation of the implemented $FEKO$ radome models.

2.1 Spherical radome

2.1.1 Single layer structure (comparison with Arvas.1990)

The following section reports the results obtained by simulating the spherical radome.

Simulation Parameters

- Frequency: $f = 3.00 \times 10^8 \ [Hz]$
- Free space wavelength: $\lambda = 1.0 \ [m]$
- EM Solver: FEM (Finite Element Method)

Radome Parameters

- Spherical radome centered in $(x, y, x) = (0, 0, 0)$
- Number of layer: $N = 1$
- Radome radius: $R \in \{0.5, 0.9\} \ [m] = \{0.5, 0.9\} \lambda$
- Radome thickness: $t = 0.1 \ [m] = \frac{\lambda}{10}$
- Radome relative permittivity: $\varepsilon \in \{1.0, 2.5, 4.0\}$

Antenna Parameters

- Short dipole centered in $(x, y, x) = (0, 0, 0)$ and directed along $\hat{\mathbf{z}}$
- Dipole length: $l_d = 8.00 \times 10^{-2} \ [m] \simeq \frac{\lambda}{12}$

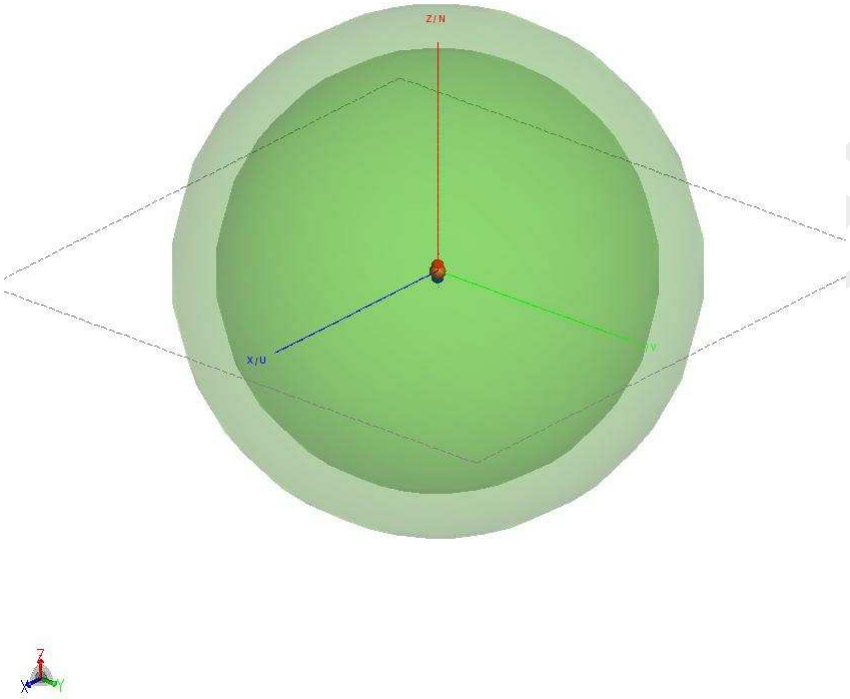

Figure 4: *(Single-layer spherical radome)* – Geometry of the radome.

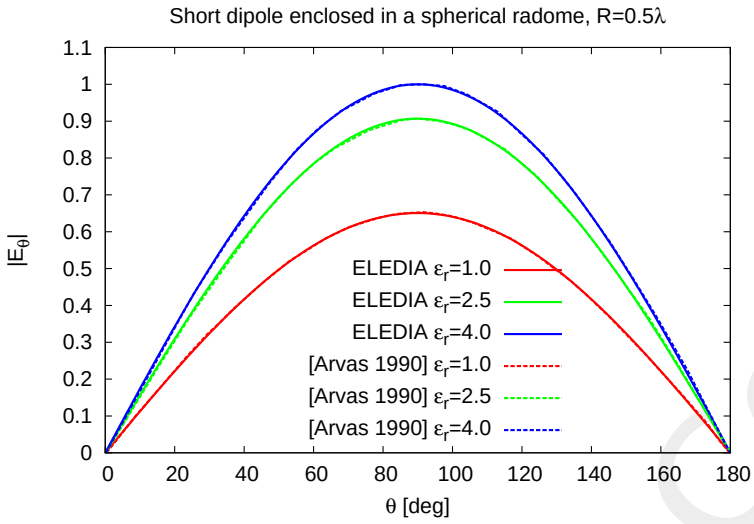

(a)

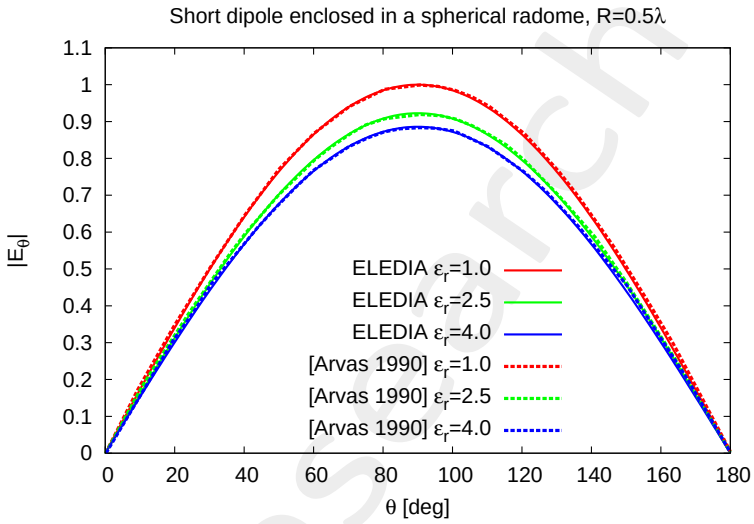

(b)

Figure 5: *(Single-layer spherical radome)* – Plot of the radiated field of the antenna in free-space and in presence of a radome with radius (a) $R = 0.5\ \lambda$ and (b) $R = 0.9\ \lambda$.

2.2 Ogive radome

2.2.1 Single layer structure (comparison with Zhao.2005)

The following section reports the results obtained by simulating the ogive radome.

Simulation Parameters

- Frequency: $f = 2.00 \times 10^8 \ [Hz]$
- Free space wavelength: $\lambda = 1.5 \ [m]$
- EM Solver: FEM (Finite Element Method)

Radome Parameters

- Number of layer: $N = 1$
- Radome length: $L = 1.75 \ [m] \simeq 1.17\lambda$
- Radome base diameter: $D = 1.6 \ [m] \simeq 1.07\lambda$
- Curvature type: $\nu = 1.449$ (tangent ogive)
- Radome thickness: $t = 7.00 \times 10^{-2} \ [m] \simeq \frac{\lambda}{21}$
- Radome relative permittivity: $\varepsilon = 2 - j$

Antenna Parameters

- Short dipole centered in $(x, y, x) = (0, 0, 0)$ and directed along $\hat{\mathbf{y}}$
- Dipole length: $l_d = 0.1 \ [m] \simeq \frac{\lambda}{15}$

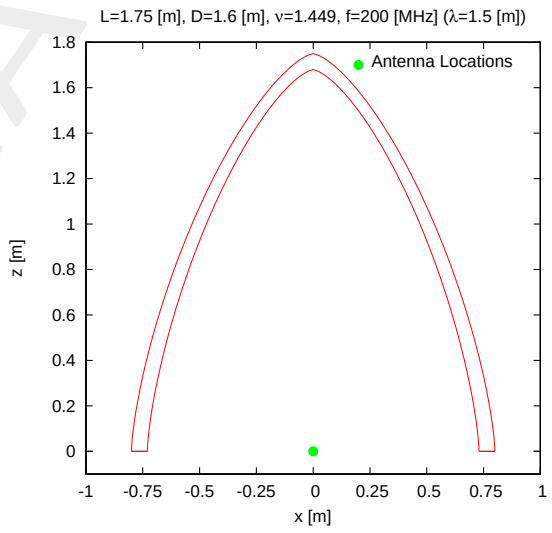

Figure 6: *(Single-layer ogive radome)* – Geometry of the radome.

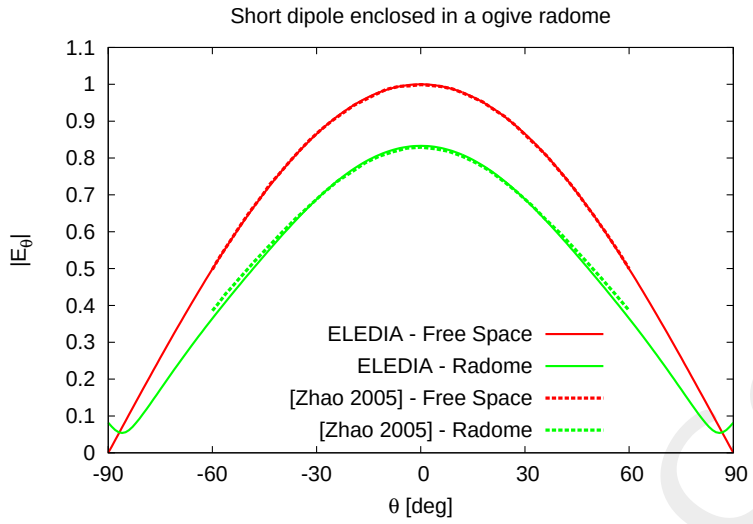

Figure 7: *(single-layer ogive radome)* – Plot of the radiated field of the antenna in free-space and in presence of the radome.

2.2.2 2-layers structure

Simulation Parameters

- Frequency: $f = 2.00 \times 10^8 \ [Hz]$
- Free space wavelength: $\lambda = 1.5 \ [m]$
- EM Solver: FEM (Finite Element Method)

Radome Parameters

- Number of layer: $N = 2$
- Radome length: $L = 1.75 \ [m] \simeq 1.17\lambda$
- Radome base diameter: $D = 1.6 \ [m] \simeq 1.07\lambda$
- Curvature type: $\nu = 1.449$ (tangent ogive)
- Radome thickness: $t = 7.16 \times 10^{-2} \ [m] \simeq \frac{\lambda}{21}$
  - $t_1 = 3.16 \times 10^{-2} \ [m]$
  - $t_2 = 4.00 \times 10^{-2} \ [m]$
- Radome relative permittivity:
  - $\varepsilon_1 = 3.72$
  - $\varepsilon_2 = 4.22$

Antenna Parameters

- Dipole centered in $(x, y, x) = (0, 0, 0)$ and directed along $\hat{\mathbf{y}}$
- Dipole length: $l_d = 0.75 \ [m] = \frac{\lambda}{2}$

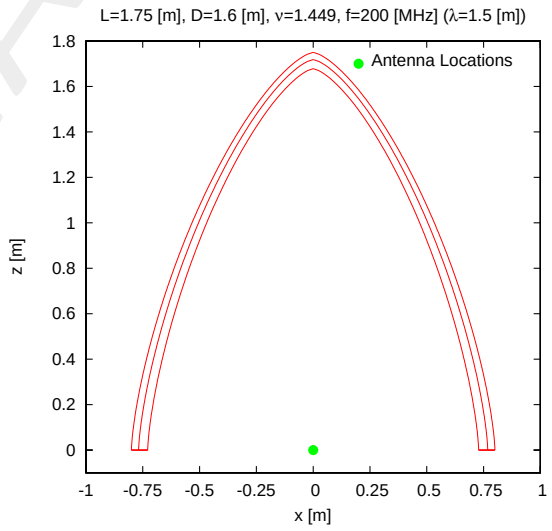

Figure 8: *(2-layer ogive radome)* – Geometry of the radome.

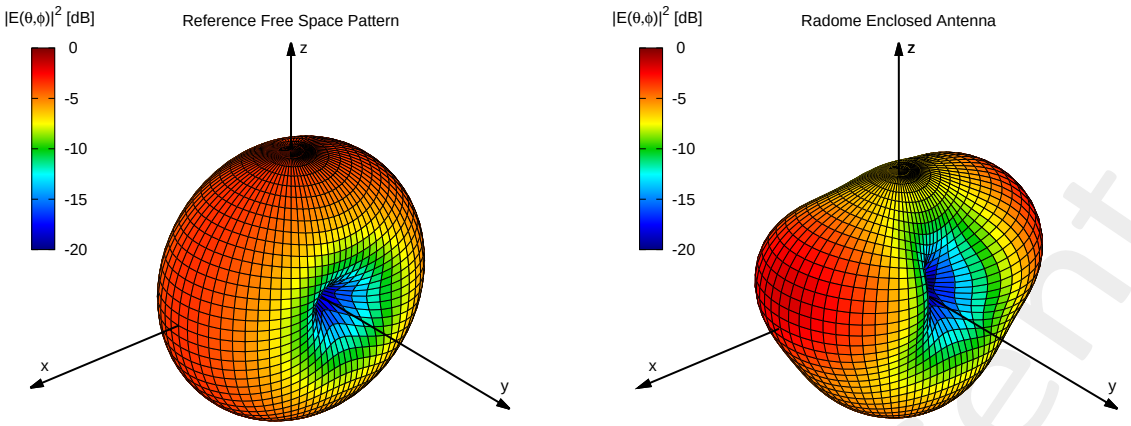

(a) (b)

Figure 9: *(2-layer ogive radome)* – 3D plot of the power pattern of the antenna (a) in free space and (b) in presence of the radome.

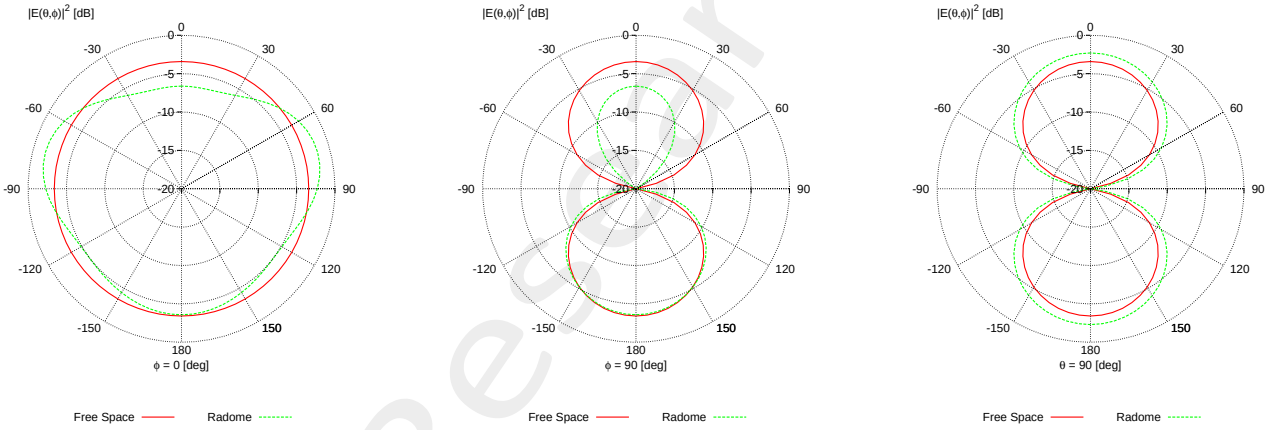

(a) (b) (c)

Figure 10: *(2-layer ogive radome)* – Polar plot of the power pattern of the antenna in free space and in presence of the radome: (a) $\phi = 0$ $[deg]$ plane, (b) $\phi = 90$ $[deg]$ plane and (c) $\theta = 0$ $[deg]$ plane.

2.2.3 3-layers structure

Simulation Parameters

- Frequency: $f = 2.00 \times 10^8 \ [Hz]$
- Free space wavelength: $\lambda = 1.5 \ [m]$
- EM Solver: FEM (Finite Element Method)

Radome Parameters

- Number of layer: $N = 3$
- Radome length: $L = 1.75 \ [m] \simeq 1.17\lambda$
- Radome base diameter: $D = 1.6 \ [m] \simeq 1.07\lambda$
- Curvature type: $\nu = 1.449$ (tangent ogive)
- Radome thickness: $t = 1.19 \times 10^{-1} \ [m] \simeq \frac{\lambda}{13}$
  - $t_1 = 4.64 \times 10^{-2} \ [m]$
  - $t_2 = 3.79 \times 10^{-2} \ [m]$
  - $t_3 = 2.76 \times 10^{-2} \ [m]$
- Radome relative permittivity:
  - $\varepsilon_1 = 4.80$
  - $\varepsilon_2 = 2.84$
  - $\varepsilon_3 = 4.89$

Antenna Parameters

- Dipole centered in $(x, y, x) = (0, 0, 0)$ and directed along $\hat{\mathbf{y}}$
- Dipole length: $l_d = 0.75 \ [m] = \frac{\lambda}{2}$

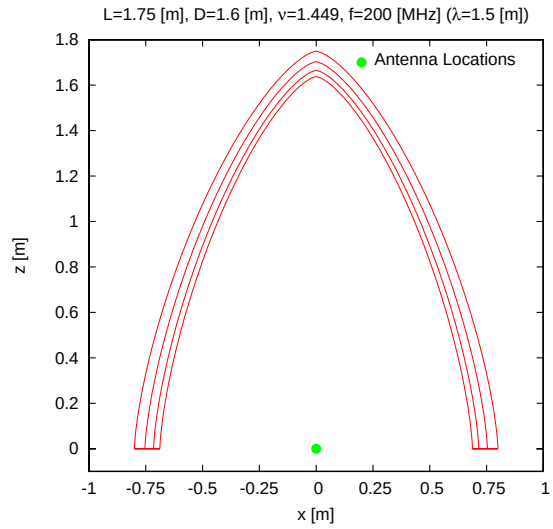

Figure 11: *(3-layer ogive radome)* – Geometry of the radome.

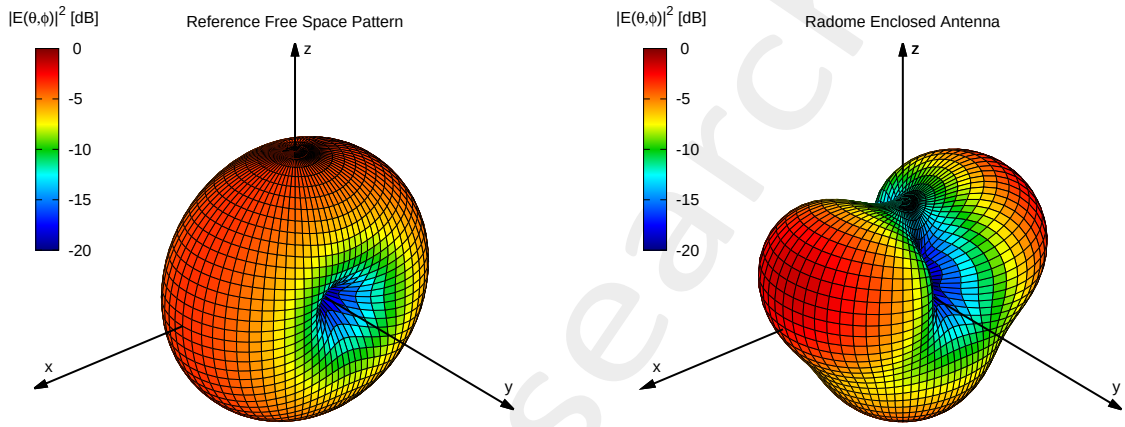

(a) (b)

Figure 12: *(3-layer ogive radome)* – 3D plot of the power pattern of the antenna (a) in free space and (b) in presence of the radome.

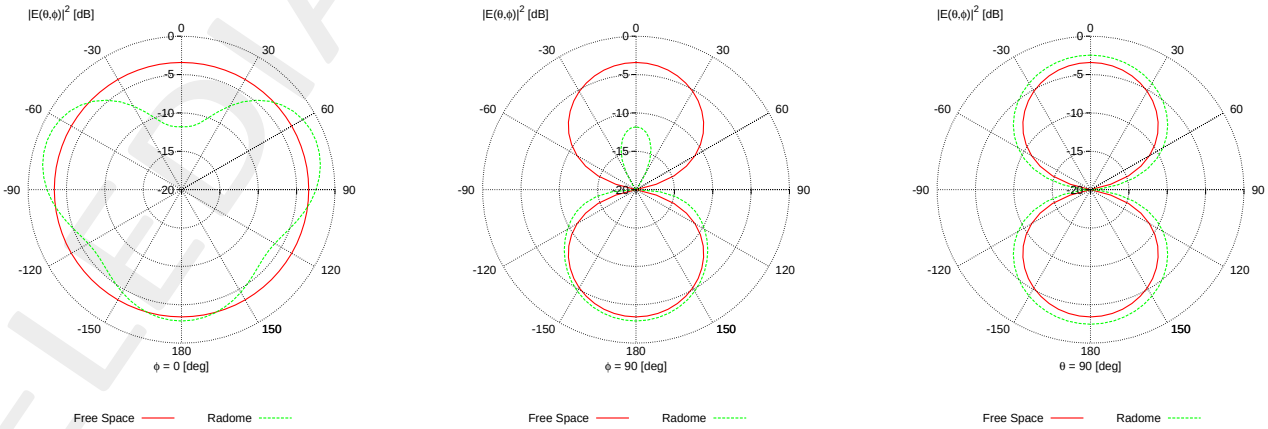

(a) (b) (c)

Figure 13: *(3-layer ogive radome)* – Polar plot of the power pattern of the antenna in free space and in presence of the radome: (a) $\phi = 0$ $[deg]$ plane, (b) $\phi = 90$ $[deg]$ plane and (c) $\theta = 0$ $[deg]$ plane.

More information on the topics of this document can be found in the following list of references.

References

[1] A. Massa, D. Marcantonio, X. Chen, M. Li, and M. Salucci, "DNNs as applied to electromagnetics, antennas, and propagation - A review," *IEEE Antennas and Wirel. Propag. Lett.,* vol. 18, no. 11, pp. 2225-2229, Nov. 2019.

[2] A. Massa, G. Oliveri, M. Salucci, N. Anselmi, and P. Rocca, "Learning-by-examples techniques as applied to electromagnetics," *Journal of Electromagnetic Waves and Applications, Invited Review Article*, pp. 1-16, 2017.

[3] G. Oliveri, M. Salucci, and A. Massa, "Towards reflectarray digital twins - An EM-driven machine learning perspective," *IEEE Trans. Antennas Propag. - Special Issue on 'Machine Learning in Antenna Design, Modeling, and Measurements*', vol. 70, no. 7, pp. 5078-5093, July 2022.

[4] M. Salucci, L. Tenuti, G. Oliveri, and A. Massa, "Efficient prediction of the EM response of reflectarray antenna elements by an advanced statistical learning method," *IEEE Trans. Antennas Propag.*, vol. 66, no. 8, pp. 3995-4007, Aug. 2018.

[5] M. Salucci, G. Oliveri, M. A. Hannan, and A. Massa, "System-by-design paradigm-based synthesis of complex systems: The case of spline-contoured 3D radomes," *IEEE Antennas and Propagation Magazine - Special Issue on 'Artificial Intelligence in Electromagnetics*,', vol. 64, no. 1, pp. 72-83, Feb. 2022.

[6] G. Oliveri, P. Rocca, M. Salucci, and A. Massa, "Holographic smart EM skins for advanced beam power shaping in next generation wireless environments," *IEEE J. Multiscale Multiphysics Comput. Tech.*, vol. 6, pp. 171-182, Oct. 2021.

[7] G. Oliveri, A. Gelmini, A. Polo, N. Anselmi, and A. Massa, "System-by-design multi-scale synthesis of task-oriented reflectarrays," *IEEE Trans. Antennas Propag.*, vol. 68, no. 4, pp. 2867-2882, Apr. 2020.

[8] M. Salucci, L. Tenuti, G. Gottardi, A. Hannan, and A. Massa, "System-by-design method for efficient linear array miniaturisation through low-complexity isotropic lenses" *Electronic Letters*, vol. 55, no. 8, pp. 433-434, May 2019.

[9] M. Salucci, N. Anselmi, S. Goudos, and A. Massa, "Fast design of multiband fractal antennas through a system-by-design approach for NB-IoT applications," *EURASIP J. Wirel. Commun. Netw.*, vol. 2019, no. 1, pp. 68-83, Mar. 2019.

[10] M. Salucci, G. Oliveri, N. Anselmi, and A. Massa, "Material-by-design synthesis of conformal miniaturized linear phased arrays," *IEEE Access*, vol. 6, pp. 26367-26382, 2018.

[11] M. Salucci, G. Oliveri, N. Anselmi, G. Gottardi, and A. Massa, "Performance enhancement of linear active electronically-scanned arrays by means of MbD-synthesized metalenses," *Journal of Electromagnetic Waves and Applications*, vol. 32, no. 8, pp. 927-955, 2018.

[12] G. Oliveri, M. Salucci, N. Anselmi and A. Massa, "Multiscale System-by-Design synthesis of printed WAIMs for waveguide array enhancement," *IEEE J. Multiscale Multiphysics Computat. Techn.*, vol. 2, pp. 84-96, 2017.

[13] A. Massa and G. Oliveri, "Metamaterial-by-Design: Theory, methods, and applications to communications and sensing - Editorial," *EPJ Applied Metamaterials*, vol. 3, no. E1, pp. 1-3, 2016.

[14] G. Oliveri, F. Viani, N. Anselmi, and A. Massa, "Synthesis of multi-layer WAIM coatings for planar phased arrays within the system-by-design framework," *IEEE Trans. Antennas Propag.*, vol. 63, no. 6, pp. 2482-2496, June 2015.

[15] G. Oliveri, L. Tenuti, E. Bekele, M. Carlin, and A. Massa, "An SbD-QCTO approach to the synthesis of isotropic metamaterial lenses" *IEEE Antennas Wireless Propag. Lett.*, vol. 13, pp. 1783-1786, 2014.

[16] A. Massa, G. Oliveri, P. Rocca, and F. Viani, "System-by-Design: a new paradigm for handling design complexity," *8th European Conference on Antennas Propag. (EuCAP 2014), The Hague, The Netherlands*, pp. 1180-1183, Apr. 6-11, 2014.

[17] P. Rocca, M. Benedetti, M. Donelli, D. Franceschini, and A. Massa, "Evolutionary optimization as applied to inverse problems," *Inverse Problems - 25 th Year Special Issue of Inverse Problems, Invited Topical Review*, vol. 25, pp. 1-41, Dec. 2009.

[18] P. Rocca, G. Oliveri, and A. Massa, "Differential Evolution as applied to electromagnetics," *IEEE Antennas Propag. Mag.*, vol. 53, no. 1, pp. 38-49, Feb. 2011.

[19] P. Rocca, N. Anselmi, A. Polo, and A. Massa, "Pareto-optimal domino-tiling of orthogonal polygon phased arrays," *IEEE Trans. Antennas Propag.*, vol. 70, no. 5, pp. 3329-3342, May 2022.

[20] P. Rocca, N. Anselmi, A. Polo, and A. Massa, "An irregular two-sizes square tiling method for the design of isophoric phased arrays," *IEEE Trans. Antennas Propag.*, vol. 68, no. 6, pp. 4437-4449, Jun. 2020.

[21] P. Rocca, N. Anselmi, A. Polo, and A. Massa, "Modular design of hexagonal phased arrays through diamond tiles," *IEEE Trans. Antennas Propag.*, vol.68, no. 5, pp. 3598-3612, May 2020.

[22] N. Anselmi, L. Poli, P. Rocca, and A. Massa, "Design of simplified array layouts for preliminary experimental testing and validation of large AESAs," *IEEE Trans. Antennas Propag.*, vol. 66, no. 12, pp. 6906-6920, Dec. 2018.

[23] N. Anselmi, P. Rocca, M. Salucci, and A. Massa, "Contiguous phase-clustering in multibeam-on-receive scanning arrays," *IEEE Trans. Antennas Propag.*, vol. 66, no. 11, pp. 5879-5891, Nov. 2018.

[24] G. Oliveri, G. Gottardi, F. Robol, A. Polo, L. Poli, M. Salucci, M. Chuan, C. Massagrande, P. Vinetti, M. Mattivi, R. Lombardi, and A. Massa, "Co-design of unconventional array architectures and antenna elements for 5G base station," *IEEE Trans. Antennas Propag.*, vol. 65, no. 12, pp. 6752-6767, Dec. 2017.

[25] N. Anselmi, P. Rocca, M. Salucci, and A. Massa, "Irregular phased array tiling by means of analytic schemata-driven optimization," *IEEE Trans. Antennas Propag.*, vol. 65, no. 9, pp. 4495-4510, Sept. 2017.

[26] N. Anselmi, P. Rocca, M. Salucci, and A. Massa, "Optimization of excitation tolerances for robust beamforming in linear arrays" *IET Microwaves, Antennas & Propagation*, vol. 10, no. 2, pp. 208-214, 2016.

[27] P. Rocca, R. J. Mailloux, and G. Toso, "GA-Based optimization of irregular sub-array layouts for wideband phased arrays desig," *IEEE Antennas and Wireless Propag. Lett.*, vol. 14, pp. 131-134, 2015.

[28] P. Rocca, M. Donelli, G. Oliveri, F. Viani, and A. Massa, "Reconfigurable sum-difference pattern by means of parasitic elements for forward-looking monopulse radar," *IET Radar, Sonar & Navigation*, vol 7, no. 7, pp. 747-754, 2013.

[29] P. Rocca, L. Manica, and A. Massa, "Ant colony based hybrid approach for optimal compromise sum-difference patterns synthesis," *Microwave Opt. Technol. Lett.*, vol. 52, no. 1, pp. 128-132, Jan. 2010.

[30] P. Rocca, L. Manica, and A. Massa, "An improved excitation matching method based on an ant colony optimization for suboptimal-free clustering in sum-difference compromise synthesis," *IEEE Trans. Antennas Propag.*, vol. 57, no. 8, pp. 2297-2306, Aug. 2009.

[31] N. Anselmi, L. Poli, P. Rocca, and A. Massa, "Design of simplified array layouts for preliminary experimental testing and validation of large AESAs," *IEEE Trans. Antennas Propag.*, vol. 66, no. 12, pp. 6906-6920, Dec. 2018.

[32] M. Salucci, F. Robol, N. Anselmi, M. A. Hannan, P. Rocca, G. Oliveri, M. Donelli, and A. Massa, "S-Band spline-shaped aperture-stacked patch antenna for air traffic control applications," *IEEE Trans. Antennas Propag.*, vol. 66, no. 8, pp. 4292-4297, Aug. 2018.

[33] F. Viani, F. Robol, M. Salucci, and R. Azaro, "Automatic EMI filter design through particle swarm optimization," *IEEE Trans. Electromagnet. Compat.*, vol. 59, no. 4, pp. 1079-1094, Aug. 2017.